



UvA-DARE (Digital Academic Repository)

From sample structure to optical properties and back

A theoretical framework for quantitative OCT and its clinical application

Almasian, M.

Publication date

2018

Document Version

Other version

License

Other

[Link to publication](#)

Citation for published version (APA):

Almasian, M. (2018). *From sample structure to optical properties and back: A theoretical framework for quantitative OCT and its clinical application*. [Thesis, fully internal, Universiteit van Amsterdam].

General rights

It is not permitted to download or to forward/distribute the text or part of it without the consent of the author(s) and/or copyright holder(s), other than for strictly personal, individual use, unless the work is under an open content license (like Creative Commons).

Disclaimer/Complaints regulations

If you believe that digital publication of certain material infringes any of your rights or (privacy) interests, please let the Library know, stating your reasons. In case of a legitimate complaint, the Library will make the material inaccessible and/or remove it from the website. Please Ask the Library: <https://uba.uva.nl/en/contact>, or a letter to: Library of the University of Amsterdam, Secretariat, P.O. Box 19185, 1000 GD Amsterdam, The Netherlands. You will be contacted as soon as possible.

APPENDIX

Published as supplementary information of:
M. Almasian et al. OCT Amplitude and Speckles statistics of discrete
random media, *Scientific Reports* (7), 2017

I – OCT GEOMETRY AND SIGNAL

Consider a medium containing hard spheres of a single size, where the position of the i 'th particle is given by $\delta(r-r_i)$; measured from a given reference particle (see Figure 1 below). These spheres can touch, but not overlap in space. This medium is imaged using an OCT system with the reference arm length ('zero delay' matched to the position of a reference particle located at depth z_b below the boundary. The scattered light is collected at the lens in the detection arm, with R the distance between reference particle and lens.

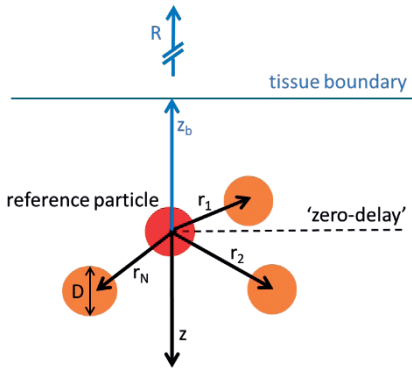


Figure 1. OCT geometry. The optical path length in the reference arm is matched to the position of a reference particle in the sample ('zero delay'). The sample consists of identical randomly placed spheres with position r_i with respect to the reference particle. The distance R is between the reference particle and the detection lens in the sample arm.

The (complex) scattered field from a volume containing N particles is given by $E_s = \sum_{i=1}^N E_i$. For identical particles (equal size and refractive index), the scattering efficiency of the individual particles is the equal, but the amplitudes and phases of the scattered fields depend on the individual particle positions. The total field at the detector is given by $E_D = E_R + \sum_{i=1}^N E_i$ where E_R is the field scattered from the reference mirror (phase-matched to the reference particle).

The real part of the (Time-Domain) OCT signal as function of depth $x(z)$ is obtained from the detector current

$$i_{DET}(z) \propto \langle |E_D|^2 \rangle = I_S(z) + I_R(z) + 2 \langle E_R \sum_{i=1}^N E_i \rangle \quad (1a)$$

$$x(z) \propto \langle E_R \sum_{i=1}^N E_i \rangle \quad (1b)$$

where the brackets denote averaging over the detector response time. I_S and I_R are intensities from sample and reference arm, respectively. Removing these DC-terms yields $x(z)$ as a cosine-modulated signal with zero-mean and non-zero variance that encodes the sample reflectivity. The imaginary part $y(z)$ is sine-modulated at the same frequency. In OCT, conventionally the amplitude $A(z) = \sqrt{x^2(z) + y^2(z)}$ is plotted in a logarithmic grayscale image. Both mean and variance of $A(z)$ are non-zero.

Figure 2 shows simulations of $x(z)$, red curve, and $A(z)$, blue curve, from a sample containing many identical, randomly placed reflectors ($N > 10$, see IV). The number of reflectors is too high to resolve their individual positions: the information about particle density and scattering strength is encoded in the variance of $x(z)$, and mean and variance of $A(z)$.

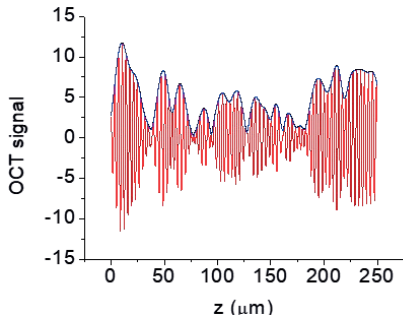


Figure 2. simulated OCT signal as function of depth of a sample containing many randomly placed reflectors. The red curve shows the real part $x(z)$ of the complex OCT signal, cosine modulated with zero mean and non-zero variance. The imaginary part $y(z)$ is not shown. The blue curve shows the amplitude $A(z)$.

II – TIME DOMAIN VS. SPECTRAL DOMAIN OCT

The analysis in I assumed detection of the OCT signal in the spatial domain (e.g. “Time-domain OCT”) rather than in the spatial frequency domain (Spectral domain OCT). The analysis however, remains the same because the time-domain and spectral domain signal are reversibly connected through a Fourier transformation. To illustrate, Figure 3A shows a simulated ‘raw spectrum’ corresponding to a single reflector, i.e. a cosine modulated in source spectrum with the position of the reflector encoded in the modulation frequency (a real signal). The result of the Fourier transform of this raw spectrum is complex. Panel B shows the result if the real part of the complex FT is calculated the signal corresponding to the red curve is obtained; if the amplitude of the complex FT is calculated the

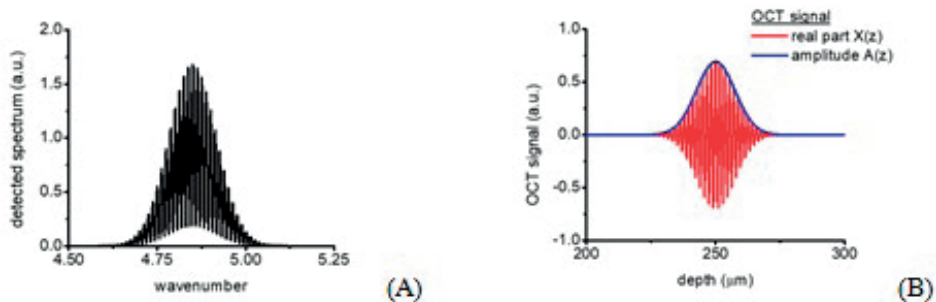


Figure 3. (A) Simulated raw spectrum in Spectral Domain OCT corresponding to a single reflector. (B) The Fourier transform of this spectrum yields a complex signal with real part $x(z)$, red curve and amplitude $A(z)$, blue curve.

envelope (blue curve) is obtained. Note that in practice, the square of the amplitude is often calculated directly from the Power Spectrum of the raw spectrum instead of via FT; and $\log(A^2)$ is converted to a grayscale image.

III – OCT SPECKLE

The (complex) scattered field from a volume containing N particles is written as $E_s = \sum_{i=1}^N E_i$. Both the amplitude and phase of E_i can be considered as random variables with no dependency on each other. Therefore, the statistics of the scattered field and according to Eq. 1B, $x(z)$ follow that of a random phasor sum as is commonly found in speckle phenomena.¹ Indeed, the random amplitudes and phases of the different scattering elements within a detection volume give rise to the static speckle pattern found in OCT images. For a large number of scatterers $x(z)$ and $y(z)$ follow a normal distribution (by the Central Limit theorem) with zero mean and non-zero variance. The amplitude $A(z) = \sqrt{x^2(z) + y^2(z)}$ is Rayleigh distributed (Eq. 2A) with mean $\langle A \rangle$ and variance σ_A^2 determined by the variance of the underlying real and imaginary components $\sigma_x^2 = \sigma_y^2 = \sigma_{x,y}^2$ (Eq. 2B):

$$p(A) = \frac{A}{\sigma^2} e^{-A^2/(2\sigma_A^2)} \quad (2A)$$

$$\langle A \rangle = \sqrt{\frac{\pi}{2}} \sigma_{x,y}^2; \quad \sigma_A^2 = \left(2 - \frac{\pi}{2}\right) \sigma_{x,y}^2 \quad (2B)$$

This also yields the familiar result that contrast in OCT, when defined as the ratio of the standard deviation over the amplitude of the OCT signal is $\sqrt{4/\pi-1} \approx 0.52$.^{2,3}

Note that when the OCT envelope is calculated as the power spectrum of a signal acquired in the spatial frequency domain, the distribution of this signal $p(P)$ follows an exponential distribution, and the contrast is unity (see II).

IV – THE REAL PART OF THE OCT SIGNAL X(Z)

The information about particle density and particle scattering strength is encoded in the variance of $x(z)$, see section I, and via Supplementary Eq. 2B also in the mean and variance of the OCT amplitude $A(z)$. In order to express $\langle A \rangle$ and σ_A^2 in terms of sample scattering properties, we first derive an expression for $x(z)$ that can be used to calculate σ_x^2 around the position of the reference particle:

$$\sigma_x^2 \equiv \langle x^2(z) \rangle - \langle x(z) \rangle^2 = \langle x^2(z) \rangle \quad (3)$$

The last equality holds because for discrete random media, the mean of $x(z)$ is zero. We assume N identical particles in the probe volume, where the scattered field in the far field of the n 'th particle can be written as⁴:

$$E_{s,n} = E_{in} \frac{f(\theta, \varphi)}{kR} e^{i\phi_n} \quad (4)$$

Where E_{in} is the input field which we assume identical for each particle under the 1st Born approximation; $f(\theta, \varphi)$ is the *scattering amplitude* of the particles (in general a complex number), ϕ_n is the phase of the scattered field which depends on the position of the particle, k is the wavenumber $k=2\pi/\lambda$ where λ is the wavelength; and R is the distance to point of evaluation. Since the distances between the particles is much smaller than the distance from the reference particle to the lens (See section I and Figure 1) we take identical R for all particles.

In the following, we express the phase of the scattered field with respect to the reference particle. The phase difference between fields scattered from 2 arbitrary particles can be written as $\Delta\phi = \mathbf{q} \cdot \mathbf{r}$ where \mathbf{q} is the wavevector $\mathbf{k}_{out} - \mathbf{k}_{in}$, $|\mathbf{q}| = 2k \sin \frac{1}{2}\theta$ with θ the scattering angle (angle of observation); and \mathbf{r} is the vector connecting both particles. Consequently, for the n 'th particle we write $\phi_n = \mathbf{q} \cdot \mathbf{r}_n$ and the computed value of x is assigned to z_b (the position of the reference particle).

Since the reference particle is matched to the reference arm, $\mathbf{q} \cdot \mathbf{r}_n$ also equals the phase difference between the scattered field and the reference arm field. This allows us to express the relative contribution of the field scattered from n 'th particle through the complex coherence function ($\mathbf{q} \cdot \mathbf{r}_n$). For an example of the real part of the complex coherence function see Figure 3B.

Finally, the scattered field contribution needs to be evaluated over the solid angle corresponding to the detection numerical aperture Ω_{NA} (i.e. of the lens in the sample arm). Combining terms, we expand Eq. 1b as:

$$x(z_b) \propto Re \left\{ \int_{\Omega_{NA}} \sum_i \gamma(\vec{q} \cdot \vec{r}_i) e^{i\vec{q} \cdot \vec{r}_i} \frac{f(\theta, \varphi)}{kR} d\Omega \right\} \quad (5)$$

Only particles within the coherence volume V_c contribute to the signal. The axial dimension of this cylindrical volume is in the order of the coherence length, the lateral radius in the order of the probe beam waist when evaluated at the focus position. Sugita et al.⁵ derived the following expression to which we adhere:

$$V_c = \frac{4\pi\omega_0^2 \sqrt{2 \ln(2)} L_c}{6} \quad (6)$$

Where L_c is the coherence length and ω_0 the 1/e intensity waist of the illuminating beam. We use this to make a further simplification of Eq. 5 by assuming that only particles within V_c contribute with equal weight to the OCT signal. Therefore we can omit the complex coherence function if we sum only over these N particles:

$$\langle x(z_b) \rangle \propto \text{Re} \left\{ \int_{\Omega_{NA}} \sum_{i=1}^N e^{i\vec{q} \cdot \vec{r}_i} \frac{f(\theta, \varphi)}{kR} d\Omega \right\} \quad (7)$$

where $N = \rho V_C$ and ρ is the average particle density (constant for the homogeneous medium assumed here).

V – MEAN SQUARED REAL OCT SIGNAL $\langle X^2(Z) \rangle$

Starting with Eq. 7 for the real part of the OCT signal we write the mean square of the real OCT signal as:

$$\langle x(z_b)^2 \rangle \propto \text{Re} \left\{ \int_{\Omega_{NA}} \left\langle \sum_{i=1}^N \sum_{j=1}^N \frac{f^2(\theta, \varphi)}{k^2 R^2} e^{i\vec{q} \cdot \vec{r}_i} e^{-i\vec{q} \cdot \vec{r}_j} \right\rangle d\Omega \right\} \quad (8)$$

This equation can be further simplified by using the definition of the differential scattering cross section of the (identical) particles, $\sigma_{\text{scat}}(\theta, \varphi) = f(\theta, \varphi)^2/k^2$ which can be taken out of the ensemble average.⁴ Further, the integration over solid angle can be written in spherical coordinates, yielding:

$$\langle x(z_b)^2 \rangle \propto \text{Re} \left\{ \int_0^{2\pi} \int_{(\pi-NA)}^{\pi} \sigma_{\text{scat}}(\theta, \varphi) \left\langle \sum_{i=1}^N \sum_{j=1}^N e^{i\vec{q} \cdot \vec{r}_i} e^{-i\vec{q} \cdot \vec{r}_j} \right\rangle \sin\theta d\theta d\varphi \right\} \quad (9)$$

For spherical particles as considered here, the differential scattering cross section does not depend on the azimuthal angle φ , and the integral over φ simply yields a factor 2π .

The double sum within chevrons $\langle \dots \rangle$ accounts for all phase differences between the particles contributing to the signal and is known from statistical physics as the structure factor.⁶ More precisely:

$$S(q) = \frac{1}{N} \left\langle \sum_{i=1}^N \sum_{j=1}^N e^{i\vec{q} \cdot \vec{r}_i} e^{-i\vec{q} \cdot \vec{r}_j} \right\rangle \quad (10)$$

Using $N = \rho V_C$ from IV where V_C is the coherence volume and ρ is the average particle density and q is the scattering vector with magnitude $2k\sin\theta/2$ (see IV). Consequently, the structure factor may be written as function of θ for convenience. Thus, and since both the differential cross section and structure factor are real numbers:

$$\langle x(z_b)^2 \rangle = \sigma_x^2(z_b) \propto \rho V_C \times 2\pi \int_{(\pi-NA)}^{\pi} \sigma_{\text{scat}}(\theta) S(\theta) \sin\theta d\theta \quad (11)$$

The equality holds based on Eq. 3.

The structure factor quantifies the effect of organization of scatters in the sample on the scattering pattern (hence its name). For discrete random media, it is closely related to the pair-correlation $g(\Delta r)$ function through a Fourier transform relationship:

$$S(q) = 1 + \rho \int g(\Delta r) e^{i\vec{q} \cdot \Delta \vec{r}} d\Delta \vec{r} \quad (12)$$

Where the pair-correlation function is interpreted the distribution of particle separations Δr . Note that both the pair-correlation function and structure factor are functions of

particle density ρ . Eq. 11 demonstrates that the variance of the real OCT signal σ_x^2 and therefore by Eq. 2B also the mean $\langle A \rangle$ and variance σ_A^2 of the OCT amplitude signal encode the scattering strength of the particles (differential cross section term) and the particle density and organization (structure factor term).

VI – INTERPRETATION AS OPTICAL COEFFICIENT

To facilitate interpretation of Eq. 11, we first note the definitions⁴ of the (total) scattering cross section (units [m²]) of a single spherical particle (Eq. 13) and scattering coefficient (units [m⁻¹]) of a medium containing such particles (Eq. 14):

$$\sigma_{\text{scat}} = 2\pi \int_0^\pi \sigma_{\text{scat}}(\theta) \sin\theta d\theta \quad (13)$$

$$\mu_s = \rho \sigma_{\text{scat}} \quad (14)$$

Comparing Eqs 11 and 13, we find that the integral is weighted with the dimensionless structure factor to account for organization in the sample. Moreover, integral boundaries are limited to the detection NA, which leads to the following cross section and coefficient ‘in the backscatter direction, within the detection NA’:

$$\sigma_{b,NA} = 2\pi \int_{(\pi-NA)}^\pi \sigma_{\text{scat}}(\theta) S(\theta) \sin\theta d\theta \quad (15)$$

$$\mu_{b,NA} = \rho \sigma_{b,NA} \quad (16)$$

Thus, at a given location in the sample, the variance of the real part of the OCT signal σ_x^2 and the variance of the envelope signal are proportional to $\mu_{b,NA}$; the mean amplitude $\langle A \rangle$ is proportional to $\sqrt{\mu_{b,NA}}$.

VI – OCT AMPLITUDE VS. DEPTH.

The numerical aperture in Eq. 15 could theoretically be expanded to collect *all* scattered light. In that case, the expressions for the scattering cross section and scattering coefficient of the discrete random medium become:

$$\sigma_{\text{scat,medium}} = 2\pi \int_0^\pi \sigma_{\text{scat,particle}}(\theta) S(\theta) \sin\theta d\theta \quad (17)$$

$$\mu_{s,medium} = \rho 2\pi \int_0^\pi \sigma_{\text{scat,particle}}(\theta) S(\theta) \sin\theta d\theta \quad (18)$$

With subscripts ‘medium’ and ‘particle’ added for emphasis but omitted henceforth.

In section I to section V it was assumed that the reference arm is matched to a reference particle at arbitrary depth z_b , and that under the 1st Born approximation, all particles within the coherence volume V_C around z_b experience the same input field. The amplitude of this illuminating field however decreases in amplitude with increasing z_b

because of losses due to light scattering and absorption (the latter is neglected in the analysis here). Likewise, part of the light scattered from V_C is scattered on the way back to the sample boundary; it is assumed that this light escapes the detection NA and does not contribute. In other words, only single scattered light is considered, for which the attenuation of intensity can be described by the Lambert-Beer law, with the μ_s of Eq. 18 as exponential decay constant. Additional depth-dependent weighting terms exist, such as the confocal point spread function (the illuminating field will be weaker if the reference particle is chosen outside the focal region) and, specifically for Spectral Domain OCT, the sensitivity-rolloff in depth. For a thorough discussion of these factors we refer to our earlier work [7] and references therein.

In a *Time-Domain* system, the moving reference arm would vary the probe depth z_b and the coherence volume around it to build up an A-line. In this case, the subscript 'b' may be dropped and the OCT A-line, defined as $\langle A(z) \rangle$ and variance $\sigma_A^2(z)$ are written as:

$$\langle A(z) \rangle_{TD} = \sqrt{\alpha_{TD}(z) \frac{\pi}{2} \mu_{b,NA} V_C \exp(-2\mu_s z)} \quad (19)$$

$$\sigma_A^2(z)_{TD} = \alpha_{TD}(z) \left(2 - \frac{\pi}{2} \right) \mu_{b,NA} V_C \exp(-2\mu_s z) \quad (20)$$

Were depth z is measured from the sample boundary. Here μ_s is given by Eq. 18, and $\mu_{b,NA}$ by the analysis in section IV. The factor 2 in accounts for scattering losses to and from the coherence volume. The term $\alpha_{TD}(z)$ accounts for scaling factors such as power-to-current efficiency of the detector, but also depth dependent losses, most notably the confocal point spread function – either using a static focus or dynamic focusing. Importantly, $\alpha_{TD}(z)$ only contains parameters related to the OCT system (not the sample) and can thus in principle be calibrated to allow for absolute measurements of $\mu_{b,NA}$.

In a *Spectral-Domain* system the zero-delay position is usually not located within the sample but at some position outside. This does not change our analysis since it will only lead to a fixed phase difference between zero delay and the reference particle. Particles will contribute to the signal as long as the distance between zero-delay and the reference particle is within the instantaneous coherence length of the system, which is determined by the spectral resolution. We therefore only slightly modify Eqs. 19 and 20:

$$\langle A(z) \rangle_{TD} = \sqrt{\alpha_{SD}(z) \frac{\pi}{2} \mu_{b,NA} V_C \exp(-2\mu_s(z-z_0))} \quad (21)$$

$$\sigma_A^2(z)_{TD} = \alpha_{SD}(z) \left(2 - \frac{\pi}{2} \right) \mu_{b,NA} V_C \exp(-2\mu_s(z-z_0)) \quad (22)$$

Were depth z is measured from zero-delay; and z_0 is the distance between zero-delay and the sample boundary. The term $\alpha_{SD}(z)$ accounts for scaling factors such as power-to-current efficiency of the detector, but also depth dependent losses, most notably the confocal point spread function and sensitivity roll-off with depth inherent to SD-OCT sys-

tems. Again, $\alpha_{SD}(z)$ only contains parameters related to the OCT system (not the sample) and can thus in principle be calibrated to allow for absolute measurements of μ_{bNA} .

VII – SCALING OF OPTICAL PROPERTIES WITH VOLUME FRACTION

Figure 4 shows the volume fraction-dependent and volume fraction-independent calculations for $\mu_{B,NA}$, μ_s , $\mu_{B,NA}/\mu_s$, anisotropy as a function of optical size ($D \cdot k_0$). For the latter calculations the structure factor is set to unity. Thus, the f_v -independent $\mu_{B,NA}/\mu_s$ and anisotropy curves do not change with volume fraction. For the f_v -dependent calculation all shown plots change with volume fraction since the structure factor, which serves as a

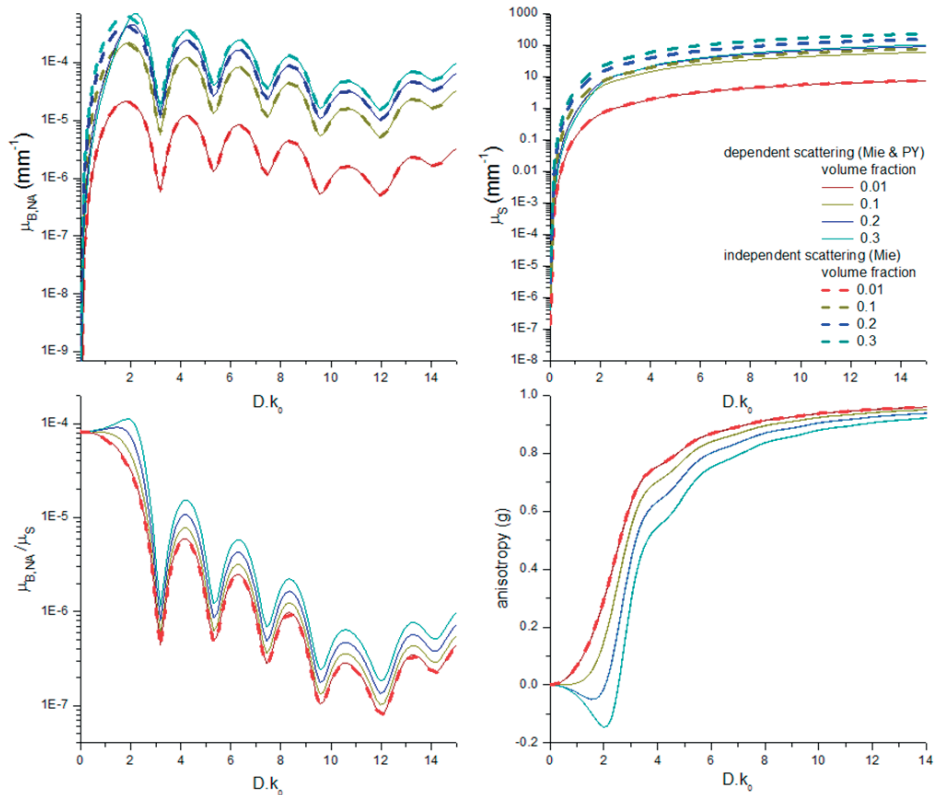


Figure 4. Calculated backscattering coefficient ($\mu_{B,NA}$) (and scattering coefficient (μ_s), $\mu_{B,NA}/\mu_s$ and anisotropy) as a function of optical particle diameter (D). k_0 , $k_0=2\pi/\lambda_{0,vacuum}$) for volume fractions of 0.01, 0.1, 0.2 and 0.3 for a center wavelength $\lambda_0 = 1300$ and bandwidth of $\Delta\lambda = 100$ nm. The solid lines are depict the concentration-dependent calculation using Eq.11 and Eq. 12. The dotted lines show the concentration-independent calculations, these are the MIE solutions. For these calculations the structure factor $S(\theta)$ in Eq. 11 and 12 from chapter 2 of this thesis is set to unity.

weighting factor on the angular scattering pattern (phase function) is a function of f_v (see also VIII).

VIII – PHASE FUNCTION CHANGE WITH CONCENTRATION/ VOLUME FRACTION

Our analysis accounts for the phase differences between the fields scattered by the individual particles in the sample. This analysis gives rise to a *structure factor* (see section V and Eq. 10) that directly influences the angular light scattering (compare Eqs. 13 and 15).

Applied to the low-NA backscattering geometry as described in our experiments ($\text{NA}=0.02$; $\theta_{\text{NA}} \sim 1^\circ$), for increasing volume fraction the NA-integrated part of the back-

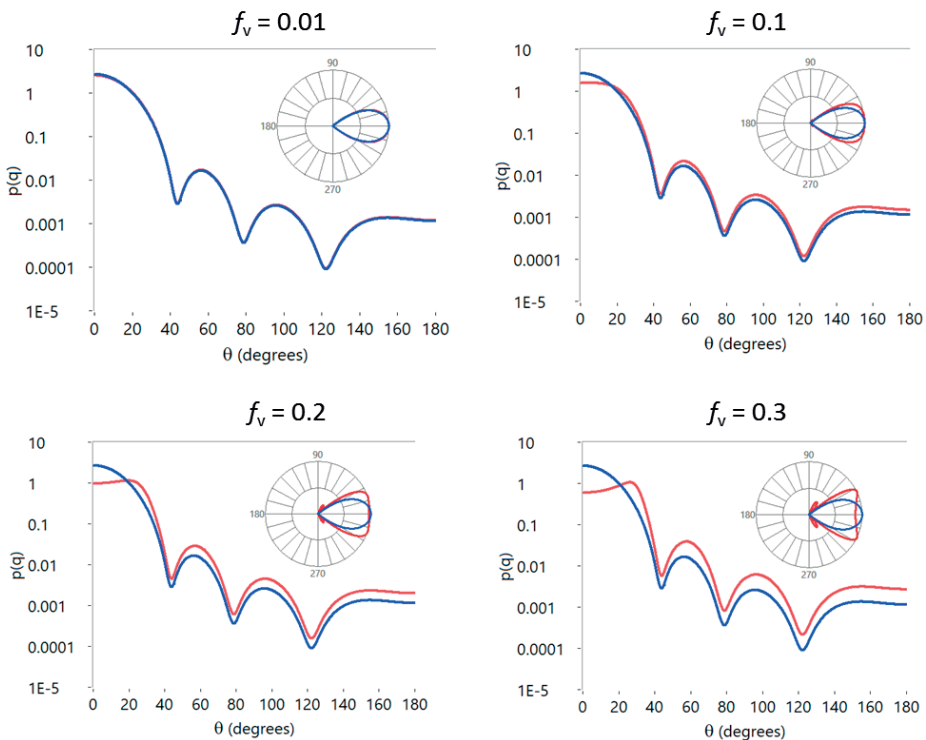


Figure 5. The phase function [4] (scattered intensity normalized on solid angle) is calculated for volume fractions of 0.01, 0.1, 0.2 and 0.3. using Mie theory ($D=0.91 \mu\text{m}$; $\lambda_0= 1300 \text{ nm}$; $n_{\text{part}} = 1.425$; $n_{\text{med}} = 1.324$) without (blue curves) and including the structure factor (red curves) as calculated from the Percus Yevick approximation. Note that our experiments did not exceed volume fractions of 0.06.

scattered intensity increases approximately linearly with volume fraction, whereas the total scattered fraction decreases with volume fraction [7].

The effect of the structure factor on angular scattering is illustrated below ($D=0.91 \mu\text{m}$; $\lambda_0= 1300 \text{ nm}$; $n_{\text{part}} = 1.425$; $n_{\text{med}} = 1.324$). We calculate the phase function, which by definition is normalized on the full solid angle. Blue curves show the phase function without inclusion of a structure factor calculated as:

$$P_{\text{Mie}}(\theta) = \frac{\sigma_s(\theta)}{2\pi \int_0^\pi \sigma_s(\theta) \sin\theta d\theta} \quad (23)$$

Where $\sigma_s(\theta)$ is the differential scattering cross section for a single particle obtained with Mie theory. Red curves show the phase function when the structure factor is included:

$$P_{\text{Mie} - \text{PY}}(\theta) = \frac{\sigma_s(\theta)S(\theta)}{2\pi \int_0^\pi \sigma_s(\theta) \sin\theta d\theta} \quad (24)$$

Where $S(\theta)$ is the Percus-Yevick structure factor appropriate for Discrete Random Media.^{6,8} All blue curves are identical. For the red curves (including the structure factor), with increasing volume fraction the amplitude of the phase function in the forward direction decreases, the amplitude in the backward direction increases, and the overall shape of the phase function becomes broader. This corresponds to a decrease of scattering anisotropy g (the average cosine of the scattering angle) as is also observed in section VII, Figure 4.

LIST OF FREQUENTLY USED SYMBOLS

μ_{OCT}	OCT attenuation coefficient
μ_{B}	Backscattering coefficient
$\mu_{\text{B,NA}}$	Backscattering coefficient within the detection numerical aperture
μ_{S}	Scattering coefficient
g	Anisotropy factor
$P(\theta)$	Phase function

REFERENCES

1. Goodman, J. W. *Speckle Phenomena in Optics: Theory and Applications*. (Roberts and Company Publishers, Englewood, 2007).
2. Hillman, T. R. *et al.* Correlation of static speckle with sample properties in optical coherence tomography. *Opt. Lett.* **31**, 190–192 (2006).
3. Karamata, B., Hassler, K., Laubscher, M. & Lasser, T. Speckle statistics in optical coherence tomography **22**, 593–596 (2005).
4. van der Hulst, H. C. *Light Scattering by Small Particles*. (Dover publications, New York, 1957).
5. Sugita, M., Brown, R. A., Popov, I. & Vitkin, A. K-distribution three-dimensional mapping of biological tissues in optical coherence tomography. *J. Biophotonics* (2017). doi:10.1002/j
6. Hansen, J.-P. & McDonald, I. R. *Theory of Simple Liquids*. (Academic Press, London, 1990).
7. Almasian, M., Bosschaart, N., van Leeuwen, T. G. & Faber, D. J. Validation of quantitative attenuation and backscattering coefficient measurements by optical coherence tomography in the concentration- dependent and multiple scattering regime. *J. Biomed. Opt.* **20**, (2015).
8. Percus, J. K. & Yevick, G. J. Analysis of Classical Statistical Mechanics by Means of Collective Coordinates. *Phys. Rev.* **110**, 1–13 (1958).

SUMMARY

Optical coherence tomography (OCT) allows 3D imaging of biological tissue with near-infrared light and a resolution around 5-15 μm and an imaging depth of about 2 mm. The light backscattered by the tissue is collected by an interferometer and converted into a cross-sectional image. In addition to morphological images, it is possible to quantify scattering parameters, *quantitative OCT*, from the OCT image using an appropriate model for the OCT signal. These scattering parameters serve as a potential additional source of information on microscopic tissue structure and organization that are not directly visible in the OCT images. Microscopic changes in tissue structure and organization are often an indication of disease. Non-invasive measurement of these changes can be a valuable clinical tool. For this reason, a large number of studies investigate the clinical application of quantitative OCT, with promising results. However, the extracted quantitative parameters strongly depend on the applied methodology, and are sensitive to the selected input parameters. In order to establish the clinical value of quantitative OCT, the extracted parameters should be reliable and robust. Furthermore, the sensitivity of these parameters to clinically relevant changes in tissue should be determined. For this reason, a standardized and validated model describing the OCT signal, and analysis method are crucial. In addition, a theoretical foundation is required that relates the quantitative parameters to microscopic tissue properties of clinical interest. The aim of this thesis is to derive and validate a model for the OCT signal and provide a robust method to extract quantitative parameters (amplitude, attenuation coefficient and speckle distribution) from OCT data and to relate these parameters to sample properties (structure, organization and flow).

Chapter 1 discusses the context and aim of this thesis and gives a brief introduction in OCT, tissue scattering and quantitative OCT. The first part of this thesis (chapter 2 and 3) provides the theoretical framework in which a model describing the OCT signal for discrete random media (DRM) is derived and validated. DRM are randomly positioned identical spherical particles for which calculations of the scattering properties are straightforward, allowing accurate analysis of the influence of sample and system properties on the OCT signal. Chapter 4 is a literature review on investigations towards clinical application of the OCT attenuation coefficient. In chapter 5 and 6 the findings from the first two chapters are applied in two *in vivo* pilot studies on the applicability of quantitative OCT during surgery. Both studies are examples of clinical cases in which non-invasive intra-operative imaging could be a valuable tool for the surgical practice. Finally, chapter 7 gives an overview of the most important findings in of the studies presented in chapters 2 to 6, followed by a discussion of the limitations and challenges concluding with suggestions for future research. Below a brief summary of chapter 2-6 is given.

In **chapter 2** we present a theoretical description of the OCT amplitude and speckle distribution for mono-disperse DRM, in which the OCT amplitude and speckle (expressed in the variance of the OCT amplitude) are linked to particle size and organization of the sample. Speckle, amplitude fluctuations between voxels in OCT images, contains information about sub-resolution structural properties of the sample. Statistical analysis of the speckle could therefore have an added value for the characterization of biological tissues. However, there is no comprehensive theoretical framework that relates OCT derived statistics to structural tissue properties. In Chapter 2 we start with the size and organization of the scattering particles, from which we derive analytical expressions for the average OCT amplitude, amplitude variance, backscattering coefficient (within the detection numerical aperture) and the scattering coefficient. In this derivation, we assume fully developed speckle and single scattered light. We show that the OCT amplitude variance (speckle) is sensitive to sub-resolution changes in size and concentration of the scattering particles. We validate the theoretical results using experimental OCT data from controlled samples of microscopic silica spheres in water and show that the experimentally determined and theoretically calculated scattering parameters correspond to each other.

In **chapter 3** we describe a comprehensive model for the OCT signal that takes into account system parameters (confocal point spread function and depth-dependent sensitivity decrease). In order to obtain reliable scattering parameters from OCT data for highly scattering tissues, consideration of the effects of multiple scattering and the non-linear relationship between the scattering coefficient and the scattering concentration (concentration-dependent scattering) is required; both effects are quantitatively included in this chapter. We verify our model with experimental OCT data from controlled samples of microscopic silica spheres in water with a wide range of scattering properties (ie scattering coefficients between 1 - 30 mm^{-1} and scattering anisotropy between 0.4-0.9). These scattering properties are calculated using the Mie-theory in combination with the Percus-Yevick structure factor to take account of concentration-dependent scattering. Multiple scattering is taken into account by the extended- Huyges-Fresnel model for OCT in combination with a priori knowledge of sample properties. We show good correspondence between the theoretical values predicted by our model and the experimentally determined values of backscatter coefficient and attenuation coefficient. We conclude that this model allows us to accurately model the backscatter coefficient and attenuation coefficient in the concentration-dependent and multiple scattering regime for mono-disperse DRM.

The attenuation coefficient is the most accessible and investigated OCT related scatter parameter to characterize tissue and distinguish between healthy and diseased tissue. **Chapter 4** is a literature study on the use of the OCT attenuation coefficient (μ_{OCT}) in (pre-) clinical studies. Models and methods to extract μ_{OCT} from OCT data as well as

the μ_{OCT} values obtained in various clinically relevant tissue samples are summarized. The overview of the reported values of μ_{OCT} suggests that although most pathologies show a change in μ_{OCT} , the difference between normal and diseased tissue is not always significant. While in some studies relative μ_{OCT} values provide added contrast, other studies combine μ_{OCT} with other OCT-derived parameters to obtain significant difference healthy and diseased tissue. Furthermore, a wide spread in μ_{OCT} values is obtained, which can be understood as a result of the use of different systems, methodologies and sample preparation. The overview of the results of these studies suggests that most pathologies show a change in μ_{OCT} , however not always significant. While in some studies relative μ_{OCT} values provide added contrast, other studies combine μ_{OCT} with other OCT-derived parameters to obtain significant difference healthy and diseased tissue. Furthermore, a wide spread in μ_{OCT} values between studies is observed, which can be understood as a result of the use of different systems, methodologies and sample preparation. It is concluded that for future research consensus on an appropriate model describing the OCT signal and a methodology to apply such model is needed.

Chapter 5 is a pilot study on the use of OCT during the neurosurgical resection of glioma. High resolution detection of cancerous tissue during glioma resection can provide a more precise resection by the surgeon and improve patient outcome. Based on result on *ex vivo* brain tissue, the use of quantitative OCT is suggested as a visual aid for the surgeon during glioma resection to distinguish glioma from normal brain tissue by intraoperative imaging. This pilot study investigates the applicability of OCT imaging during the neurosurgical resection of glioma in combination with automated quantitative analysis. For this purpose, 3D OCT datasets were collected *in vivo* in five patients during the standard surgical procedure. OCT data was collected before the resection (cortical) and after partial resection of the tumor (subcortical) from both glioma and normal brain tissue. These areas were selected by the neurosurgeon by means of visual inspection of the brain tissue, as well as pre-operative MRI images. Next, μ_{OCT} and speckle contrast values from the OCT data were quantified using an automated and validated algorithm. From the results we conclude that the proposed method for quantitative *in vivo* OCT of the cortical brain tissue is feasible during glioma resection. The applicability for sub-cortical areas was limited due to surgical limitations and the current dimensions of the OCT probe, which has led to a low quality of the OCT data. Although the found μ_{OCT} values are close to the previously reported *ex vivo* study, further research is needed to determine the potency of μ_{OCT} to distinguish glioma from normal brain tissue. To this end, OCT images and gold standard histology should be matched as close as possible in future studies.

In **chapter 6** we investigate the application of OCT as an intraoperative imaging technique for the detection of blood flow during esophageal cancer surgery with gastric tube reconstruction. Change in perfusion of the gastric tube tissue can lead to isch-

emia, resulting in high morbidity and mortality. Anastomotic leakage (incidence 5-20%) is one of the most serious complications after esophageal resection with gastric tube reconstruction. Optical imaging techniques can provide minimally invasive and real-time visualization that can be used in intraoperative environments. By implementing an optical technique for detection of blood flow during surgery, perfusion can be imaged and quantified, then, if necessary, the perfusion can be improved by surgical intervention or administration of medication. The feasibility of visualization of the *in vivo* microcirculation of the gastric tissue during operations of patients with esophageal cancer by means of detection of blood flow based on the speckle contrast from M-mode OCT images is demonstrated. The percentage of pixels with a speckle contrast value indicative of flow was quantified as an objective parameter to assess presence of blood flow at 4 sites on the reconstructed gastric tube. This chapter demonstrates that OCT can be used for direct imaging of blood flow during surgery and could therefore help improve surgical outcomes for patients.

Finally, in **chapter 7** main findings, limitations and challenges of the research presented in this thesis are discussed, followed by suggestions for future research.

SAMENVATTING

Optische coherentietomografie (OCT) is een beeldvormingstechniek die het mogelijk maakt om door middel van licht 3D-beelden van biologische weefsels te maken met een resolutie van rond de 5-15 μm en een dieptebereik van ongeveer 2 mm. Het terugverstrooide licht wordt opgevangen door een interferometer en omgezet in een dwarsdoorsnede van het weefsel, waarin weefselstructuren en morfologie zichtbaar zijn. Naast het maken van beelden is het mogelijk om verstrooiingsparameters uit de OCT-beelden te kwantificeren door gebruik te maken van een geschikt model voor het OCT-signaal. Deze verstrooiingsparameters dienen als een potentiële aanvullende bron van informatie over microscopische weefseleigenschappen die niet direct zichtbaar zijn in de OCT-beelden. Microscopische veranderingen in weefseleigenschappen, zoals (sub-) cellulaire veranderingen in structuur en organisatie, zijn vaak een indicatie voor het ontwikkelen van ziekte en daarom interessant. Het niet-invasief meten van deze (sub-)cellulaire veranderingen kan in sommige klinische situaties zeer waardevol zijn. De veelbelovende resultaten van een groot aantal studies vormen de motivatie voor het voortzetten van dit onderzoek. Om de klinische waarde van de gekwantificeerde verstrooiingsparameters te bepalen, moeten deze parameters allereerst betrouwbaar en robuust zijn. Echter is de bepaling van deze verstrooiingsparameters sterk afhankelijk van het toegepaste model voor het OCT-signaal en de, op het moment, vaak op menselijk input berustende analysemethode. Hierom zijn een gestandaardiseerd en gevalideerd model voor het OCT-signaal en analysemethode cruciaal. Bovendien is er een theoretische onderbouwing nodig die de verstrooiingsparameters relateert aan klinisch relevante microscopische weefseleigenschappen. Het hoofddoel van dit proefschrift is het afleiden en valideren van een model voor het OCT-signaal en een robuuste methode om kwantitatieve verstrooiingsparameters (terugverstrooiingscoëfficiënt, attenuatie coëfficiënt en speckledistributie) uit OCT-data te bepalen en te relatere aan sample-eigenschappen (structuur, organisatie en doorbloeding).

Hoofdstuk 1 is een introductie in de OCT-techniek, verstrooiing en kwantitative OCT. Daarnaast wordt de context rond de hoofdvraag van dit proefschrift geschetst en worden de onderzoeksthema's per hoofdstuk kort besproken. Het eerste deel van dit proefschrift (**hoofdstuk 2 en 3**) vormt het theoretische kader waarin een model voor het OCT-signaal voor *discrete random media* (DRM) wordt afgeleid en gevalideerd. DRM zijn willekeurig gepositioneerde identieke bolvormige deeltjes waarvoor berekeningen van de verstrooiingseigenschappen eenvoudig zijn. Hierdoor is een nauwkeurige analyse van de invloed van sample-eigenschappen en systeemeigenschappen op het OCT-signaal mogelijk.

In **hoofdstuk 2** presenteren we een theoretische beschrijving van de OCT-amplitude en speckle distributie voor monodisperse DRM, waarin OCT-amplitude en speckle

(uitgedrukt in de variantie van de OCT-amplitude) worden gelinkt aan deeltjesgrootte en organisatie van de sample. Speckle, oftewel amplitudeschommelingen tussen de voxels in OCT-beelden, bevat namelijk informatie over sub-resolutie weefseleigenschappen. Statistische analyse van de speckle zou daarom een toegevoegde waarde kunnen hebben voor karakterisatie van biologische weefsels. Er is echter nog geen uitgebreid theoretisch kader dat OCT-speckle-statistieken relateert aan sample-eigenschappen. In dit hoofdstuk beginnen we onze afleiding van het OCT-signaal bij de grootte en concentratie van de verstrooiende deeltjes, waaruit we analytische uitdrukkingen afleiden voor het OCT-amplitudegemiddelde, amplitudevariantie, terugverstrooiingscoëfficiënt en de verstrooiingscoëfficiënt. We gaan bij deze afleiding uit van volledig ontwikkelde speckle en enkelvoudig verstrooid licht. We laten zien dat de OCT-amplitudevariantie (speckle) gevoelig is voor subresolutie veranderingen in grootte en concentratie van de verstrooiende deeltjes. We valideren de theoretische resultaten met behulp experimentele OCT-data van gecontroleerde samples van microscopische silicabollen in water en laten zien dat de experimenteel bepaalde en theoretisch berekende verstrooiingsparameters goed overeenkomen met elkaar.

In **hoofdstuk 3** beschrijven we een uitgebreid model voor het OCT-signaal waarin rekening wordt gehouden met systeemp parameters (confociaal functie en diepteafhankelijke gevoeligheidsafname). Om betrouwbare verstrooiingsparameters te verkrijgen uit OCT-data voor sterk verstrooiende weefsels is een nauwkeurige afweging van de effecten van meervoudige verstrooiing en concentratie-afhankelijke verstrooiing vereist; beide effecten worden kwantitatief meegenomen in de berekening van de verstrooiingseigenschappen van onze samples. We verifiëren ons model met experimentele OCT-data van gecontroleerde samples van microscopische silicabollen in water met een groot bereik van verstrooiingseigenschappen (nl. verstrooiingscoëfficiënten tussen $1 - 30 \text{ mm}^{-1}$ en verstrooiingsanisotropie tussen $0,4-0,9$). Deze verstrooiingseigenschappen worden berekend met behulp van de Mie-theorie in combinatie met de Percus-Yevick-structurfactor om rekening te houden met concentratieafhankelijke verstrooiing. De meervoudige verstrooiing wordt berekend door gebruik te maken van het extended-Huygens Fresnel (EHF) model in combinatie met a priori kennis van de sample-eigenschappen. We tonen een uitstekende overeenkomst aan tussen de door ons model voorspelde theoretische waarden en de experimenteel bepaalde waarden van terugverstrooiingscoëfficiënt en attenuatiecoëfficiënt. We concluderen dat dit model ons in staat stelt om de terugverstrooiingscoëfficiënt en attenuatiecoëfficiënt nauwkeurig te modelleren in het concentratie-afhankelijke en meervoudige verstrooiingsregime voor monodisperse DRM.

Hoofdstuk 4 is een literatuurstudie naar het gebruik van de OCT-attenuatiecoëfficiënt (μ_{OCT}) in (pre-) klinische onderzoeken. De attenuatiecoëfficiënt is de meest toegankelijke en onderzochte OCT-gerelateerde verstrooiingsparameter om weefsel te karakteriseren

en onderscheid te maken tussen gezond en ziek weefsel. In dit hoofdstuk wordt een overzicht gegeven van de in literatuur beschreven modellen en methoden om μ_{OCT} uit de OCT-data te kwantificeren. Daarnaast wordt er een overzicht gegeven van de verkregen μ_{OCT} waarden van verschillende klinisch relevante weefsels. De in de literatuur beschreven resultaten laten dat er een verandering in μ_{OCT} waargenomen wordt bij pathologisch weefsel ten opzichte van gezond weefste. Echter is deze verandering niet altijd significant en is er een grote spreiding in μ_{OCT} waarden. De spreiding in μ_{OCT} waarden kan worden begrepen als het resultaat van het gebruik van verschillende OCT-systemen, modellen en samplevoorbereiding. Uit dit hoofdstuk komt naar voren dat toekomstig onderzoek grotendeels zal profiteren van consensus over een geschikt model voor het OCT-signaal, standaardisatie van data-analyse en samplevoorbereiding, en het gebruik van kalibratiesamples.

In **hoofdstuk 5 en 6** worden de bevindingen van de eerste twee hoofdstukken toegepast in twee *in vivo pilotstudies* naar de toepasbaarheid van kwantitatieve OCT tijdens operaties. Beide onderzoeken zijn voorbeelden van klinische casussen waarin niet-invasieve intra-operatieve beeldvorming een zeer waardevol hulpmiddel zou kunnen zijn in de chirurgische praktijk. In **hoofdstuk 5** onderzoeken we het gebruik van OCT tijdens de neurochirurgisch resectie van glioma in een pilotstudie. Hogeresolutie detectie van kankerweefsel tijdens gliomaresectie kan zorgen voor een preciezere resectie door de chirurg. In de literatuur wordt kwantitatieve OCT voorgesteld als een visueel hulpmiddel voor de chirurg tijdens gliomaresectie om door middel van intra-operatieve beeldvorming glioma van normaal hersenweefsel te onderscheiden. De pilotstudie in hoofdstuk 5 onderzoekt de toepasbaarheid van OCT-beeldvorming tijdens de neurochirurgisch resectie van glioma in combinatie met geautomatiseerde kwantitatieve analyse. Hiervoor zijn *in vivo* 3D OCT-data verzameld tijdens de standaard chirurgische procedure van gliomaresectie in vijf patiënten. OCT-data is verzameld vóór de resectie (corticaal) en na gedeeltelijke resectie van de tumor (subcorticaal); in beide gevallen van zowel gliomaweefsel als van normaal hersenweefsel. Deze gebieden zijn geselecteerd door de neurochirurg d.m.v. visuele inspectie van het hersenweefsel, evenals pre-operatieve MRI-afbeeldingen. Vervolgens zijn μ_{OCT} en speckle contrast waarden uit de OCT-data gekwantificeerd met behulp van een geautomatiseerd en gevalideerd algoritme. Uit de resultaten van deze pilotstudie concluderen we dat de voorgestelde methode voor kwantitatieve *in vivo* OCT van het corticaal hersenweefsel tijdens de gliomaresectie haalbaar is. De toepasbaarheid voor subcorticale gebieden is gelimiteerd vanwege chirurgische beperkingen en de huidige afmetingen van de OCT-probe, wat heeft geleid tot een lage kwaliteit van de OCT-data. Hoewel de gevonden μ_{OCT} waarden dicht bij de eerder gerapporteerde *ex vivo* studie liggen, is verder onderzoek nodig om het de onderscheidend potentie van μ_{OCT} tussen glioom en normaal hersenweefsel te bepalen. Hiervoor is een zo goed mogelijk match tussen OCT-beelden en goudenstandaard histologie cruciaal.

In **hoofdstuk 6** onderzoeken we het gebruik van OCT als een intra-operatieve beeldvormingstechniek voor detectie van doorbloeding tijdens slokdarmkankeroperaties met maagbuisreconstructie. Verandering in perfusie van het maagbuisweefsel kan leiden tot ischemie, met een hoge morbiditeit en mortaliteit tot gevolg. Anastomotische lekkage (incidentie 5-20%) is een van de ernstigste complicaties na slokdarmresectie met maagbuisreconstructie. Optische beeldvormingstechnieken kunnen voorzien in minimaal invasieve en real-time visualisatie die gebruikt kan worden in intra-operatieve omgevingen. Door het implementeren van een optische techniek voor detectie van doorbloeding tijdens chirurgie kan perfusie worden afgebeeld en gekwantificeerd. Vervolgens kan, indien nodig, de perfusie worden verbeterd door een chirurgische ingreep of door toediening van medicatie. De haalbaarheid van visualisatie van de *in vivo* microcirculatie van het maagweefsel tijdens operaties van patiënten met slokdarmkanker door middel van detectie van doorbloeding op basis van het speckle contrast uit M-mode OCT-beelden wordt gedemonstreerd. Het percentage pixels met een speckle contrast waarde dat indicatief is voor stroming werd gekwantificeerd als een objectieve parameter om de doorbloeding op vier plaatsen op de gereconstrueerde maagbuis te beoordelen. In dit hoofdstuk wordt aangetoond dat OCT kan worden gebruikt voor directe beeldvorming van de bloedstroom tijdens chirurgie en daarom zou kunnen helpen bij het verbeteren van chirurgische uitkomsten voor patiënten.

Tot slot geeft **hoofdstuk 7** een overzicht van de belangrijkste bevindingen uit dit proefschrift en worden er suggesties gedaan voor toekomstig onderzoek.

LIST OF PUBLICATIONS

Part of this thesis

- M. Almasian, N. Bosschaart, T.G. van Leeuwen, D.J. Faber, *Validation of quantitative attenuation and backscattering coefficient measurements by optical coherence tomography in the concentration-dependent and multiple scattering regime*, Journal of Biomedical Optics (20), 2015
- M. Almasian, T.G. van Leeuwen, D.J. Faber, *OCT Amplitude and speckle statistics in discrete random media*, Scientific reports (7), 2017
- S.M. Jansen*, M. Almasian*, L.S. Wilk, D.M. de Bruin, M.I. van Berge Henegouwen, S.D. Strackee, P.R. Bloemen, S.L. Meijer, S.S. Gisbertz, T.G. van Leeuwen, *Feasibility of optical coherence tomography (OCT) for intra-operative detection of blood flow during gastric tube reconstruction*, Sensors (18), 2018
- M. Almasian, L.S. Wilk, P.R. Bloemen, T.G. van Leeuwen, M. ter Laan, M.C.G. Aalders, *Pilot feasibility study of in vivo intraoperative quantitative optical coherence tomography of human brain tissue during glioma resection* (submitted)

Other publications

- M. Almasian, J. Grzetic, G. Berden, B. Bakker, W. J. Buma, J. Oomens. *Gas-phase infrared spectrum of the anionic GFP-chromophore*, International Journal of Mass Spectrometry (330), 2012
- M. Almasian, J. Grzetic, J. van Maurik, J. D. Steill, G. Berden, S. Ingemann, W. J. Buma, J. Oomens. *Non-equilibrium isomer distribution of the gas-phase photoactive yellow protein chromophore*, The journal of physical chemistry letters. Lett. (3), 2012
- B. Bedussi, M. Almasian, J. de Vos, E. van Bavel, E. N. T. P. Bakker, *Paravascular spaces at the brain surface: Low resistance pathways for cerebrospinal fluid flow*, Journal of Cerebral Blood Flow & Metabolism (38), 2018
- B. G. Muller, R. A. A. van Kollenburg, A. Swaan, E. C. H. Zwartkuis, M. J Brandt, L. S. Wilk, M. Almasian, A. W. Schreurs, D. J. Faber, L. R. Rozendaal, A. N. Vis, J. A. Nieuwenhuijzen, J. R. J. A. van Moorselaar, J. J. M. C. H. de la Rosette, D. M. de Bruin, T. G. van Leeuwen. *Needle based optical coherence tomography for the detection of prostate cancer: a visual and quantitative analysis in 20 patients*, Journal of Biomedical Optics (23), 2018

- A. Swaan, B. G. Muller, L. S. Wilk, M. Almsian, R. A. A. van Kollenburg, E. C. H. Zwartkruis, L. R. Rozendaal, D. M. de Bruin, D. J. Faber, T. G. van Leeuwen, M. B. Van Herk. *One-to-one registration of en-face optical coherence tomography attenuation coefficients with histology of a prostatectomy specimen* (submitted)

In preparation

- M. Almasian*, P. Gong*, D. J. Faber, G. van Soest, D.M. de Bruin, D.D. Sampson, T. G. van Leeuwen. *Parametric imaging of attenuation by optical coherence tomography: a review of models, methods and clinical applications*
- M.Almasian, T.G. van Leeuwen, D.J. Faber, *Numerical Aperture dependence of the OCT attenuation coefficient*
- A. A. Meesters, M. J. Nieboer, M. Almasian, M. A. de Rie, R. M. Verdaasdonk, Albert Wolkerstorfer. *Influence of various penetration enhancement techniques on ablative fractional laser assisted delivery of indocyanine green in the skin*

PORTFOLIO

Portfolio	Mitra Almasian
PhD period	November 2012- August 2018
Location	Department of biomedical engineering and physics, UMC location AMC, Amsterdam
Supervisor	prof. A. G. J. M. van Leeuwen, prof. M. C. G. Aalders
Co-supervisor	dr. D. J. Faber

COURSES

Our Future Leaders, the Recess College, Module 1 and 2, 2016 4 ECTS
"...for young adult participants who wish to work on the dynamics of organisations followed by personal development coaching. They will gain support in understanding organisations as these affect them and their capacity to get a job and develop their career, with a personal debrief in order to understand their own reactions and behaviours."

E-Science, AMC Graduate School 2014 0.3 ECTS
"The aim of this course is to bring attention to new approaches that can be used for handling large-scale data in biomedical research, including processing, data management and collaboration."

Scientific Writing, AMC Graduate School 2013 1.5 ECTS

AMC World of Science, AMC Graduate School 2013 0.7 ECTS
"The aim of this course is to provide the fundamental knowledge and skills needed for scientific research, and to prepare AMC PhD candidates for their thesis at the AMC."

6th International Graduate Summer School - Biophotonics '13 2013 3 ECTS
Poster: *i-OCT: Integrated smart Optics for low cost super resolution OCT*

Optics and Optical Quality of the Human Eye 2013 0.5 ECTS
SPIE Photonics West, course: SC702, by prof. A. Roorda

ORAL PRESENTATIONS

- OCT of the Reconstructed Gastric Tube, SPIE ECBO 2017, Munich, Germany (Invited talk)
- OCT Signal and Speckle distribution of Discrete Random Media, SPIE ECBO 2017, Munich, Germany
- Tailored Radiative Transport Modelling – Morphology-Based Computation, NICAS Match day, 2017, Rijksmuseum Amsterdam, NL
- Quantification of Numerical Aperture-Dependence of the OCT Attenuation Coefficient, SPIE Photonics West 2016, San Francisco, US. First author: L. Peinado
- Quantitative OCT for Tissue Characterization, COST ACTION European Network for Skin Cancer Detection using Laser Imaging, 2016, Barcelona, Spain (Invited talk)
- From Light Scattering to Pathology & Quantative OCT, COST ACTION BM1205 European Network for Skin Cancer Detection using Laser Imaging, 2016, Split, CROATIA (program committee member)
- OCT Model of Discrete Random Media Links Optical Properties to Micro-scale Sample Organization, SPIE ECBO 2015, Munich, Germany
- Is there Information in the Noise? OCT Speckle Reflects on Clinically Relevant Tissue Properties, COST ACTION BM1205: European Network for Skin Cancer Detection using Laser Imaging, 2015, Porto, Portugal (Invited talk)
- OCT Signal Model for Discrete Random Media, SPIE Photonics West 2015, San Francisco, US
- OCT of the Reconstructed Gastric Tube, SPIE ECBO 2015, Munich, Germany (Invited talk)
- Linking micro-scale tissue organization to OCT-derived scattering properties, Laser-Lab Amsterdam symposium, 2014, Amsterdam, NL (Invited talk)

CONFERENCE POSTERS

- Model for Optical Coherence Tomography Derived Optical Properties, Gordon Research Conference 2016, Holderness, US
- Optical Coherence Tomography of Bi-disperse Discrete Random Media, SPIE Photonics West 2016, San Francisco, US
- Tissue Properties from OCT Speckle Statistics, Gordon Research Conference 2014, Mount Snow, US
- I-OCT: integrated smart optics for super resolution OCT, annual project update, IOP Photonic Devices Symposium, The Netherlands, annually

Parameters of Esteem

Enlighten Your Research 4, SURF, NWO, NL e-Science Centre 2013

Title: A Light path for Optical Coherence Tomography Imaging

“For this edition researchers from any discipline and with any level of technical expertise were invited to submit a proposal with challenging data questions.”

Extracurricular activities

- Peer facilitation training, Recess college 2017-2018
- Board member AMC PhD association 2013-2015
- Committee member AMC PhD Science Night 2014

Student coaching/mentoring

- Gabriela Diaz, Interpretation of OCT Scans of Multi-layer Varnishes on Oil Painting Reconstructions, Materials Science and Engineering, Northwestern University (2017)
- Nick Hendriks, Extraction of the OCT attenuation coefficient: a comparison between the curve-fitting and depth-resolved method, Hogeschool Utrecht Master of education physics (2015)
- Lukas Kramer, Eye motion tracker, Technical University Delft and TNO (2015)
- Susanne Groothuis, Literature review on adaptive optics optical coherence tomography, Faculty of Science, University of Amsterdam (2014)

ABOUT THE AUTHOR

Mitra was born in Teheran, Iran on May 14th 1985. After moving to the Netherlands, she completed secondary school in 2004 at the Oostvaarders College in Almere, the Netherlands. She obtained a bachelor's degree in the interdisciplinary bachelor's program bèta-gamma with a major in Chemistry in 2009 at the University of Amsterdam. Mitra continued her studies at the University of Amsterdam with a master in Physical Sciences from which she graduated in 2012, with a thesis titled "IR spectroscopic study of the isolated PYP and GFP chromophores", based on research performed at FOM Rijnhuizen institute, under supervision of prof. Jos Oomens. At the end of 2012 she joined the department of Biomedical Engineering and Physics at the Academic Medical Center in Amsterdam. Under the supervision of prof. Ton van Leeuwen she worked on multiple projects on quantitative OCT. The results of her research are presented in this thesis.



DANKWOORD

Na een *rollercoaster ride* met *ups and downs*, typ ik nu de laatste woorden van dit boekje dat je in je handen hebt. Het was een mooie, leerzame reis en ik ben iedereen bedankbaar die op welke manier dan ook heeft bijgedragen aan het tot stand komen van dit proefschrift.

Dit onderzoek zou niet mogelijk zijn zonder mijn (co-)promotores: Prof. Ton van Leeuwen, Prof. Maurice Aalders en dr. Dirk Faber. Bedankt voor het mogelijk maken van dit onderzoek en voor de supervisie tijdens het uitvoeren van dit onderzoek.

Beste Ton, bedankt voor je vertrouwen en begeleiding tijdens dit promotieonderzoek. Ik ben dankbaar dat ik op jouw afdeling aan mijn promotieonderzoek heb kunnen werken. Bedankt voor de ruimte en mogelijkheid die je mij hebt gegeven om met verschillende onderzoeken en samenwerkingen bezig te zijn. Jouw wetenschappelijke inzichten op de verschillende uitdagingen, waar we vaak tijdens de *rebuttal* fase tegenaan liepen, waren altijd erg waardevol en inspirerend.

Beste Maurice, bedankt voor je begeleiding en motivatie tijdens dit promotieonderzoek. Het schrijven van papers en dit boekje zijn een stuk soepeler gegaan dankzij jouw inzichten en kritische vragen. Daar heb ik enorm veel van geleerd, dank daarvoor. Ik ben je dankbaar dat je me hebt geïntroduceerd bij het NICAS en het *cultural heritage* onderzoek, waar we hele gave metingen hebben gedaan.

Beste Dirk, bedankt voor je vertrouwen in mij om dit onderzoek uit te voeren en voor al je input waarop dit onderzoek gebaseerd is. Daarnaast wil ik je bedanken voor alle uitleg en discussies over de theorie. De steeds weer terugkomende discussies over afhankelijke en meervoudige verstrooiing, *speckle* en systeem parameters waren zeer de moeite waard en hebben hun waarde bewezen bij het tot stand komen van dit boekje.

Ook wil ik de patiënten bedanken. Zonder medewerking van de patiënten zou een deel van dit onderzoek en de translatie van het lab naar de kliniek niet mogelijk zijn.

Dear members of the thesis committee, thank you all for taking the time and your interest to be part of this committee and for reading and assessing this thesis.

Gijs, wat toevallig dat we tegelijkertijd in Perth zaten. Bedankt voor je interesse in mijn onderzoek en de discussies over *speckle*.

I would like to thank everyone that I had the pleasure of working with during my PhD, both in the Netherlands and in Perth, Australia. Dear David Sampson thank you for inviting me to your lab at the UWA. I had such a good time in Perth, I'm grateful for the hospitality from everyone I worked with and met in Perth. Moreover, I would like to thank all the co-authors who have contributed to the chapters presented in this thesis. It was also a pleasure collaborating with the Departments of Dermatology and Ophthalmology, TU Delft, TNO, Rijksmuseum and NICAS. Although not all of the results from these col-

laborations made their way into this thesis they were extremely valuable, stimulating and enjoyable.

A big thanks to all my colleagues and friends from the Biomedical Engineering & Physics Department: you all created such a lovely environment to work in. I had a blast working with you all and enjoyed the coffee breaks, conferences, Friday afternoon drinks, lab-uitjes and karaoke bar sessions. Anouk, Abel, Xu, Lorena, Richelle, Nienke, Annemarie, Edwin, Frank, Mieke, Ilaria, Mathijs and Rob. Thank you for your scientific advice, support and friendship. Judith and Angela, bedankt voor jullie hulp bij alle labgerelateerde vragen. Het was altijd fijn om "scheikundige inzichten" uit te wisselen. Bea, thank you for your amazing attitude towards life, and of course your humor. I enjoyed our talks, drinks and concerts, from which the latter amazingly led to a collaboration on a paper and most importantly, getting some OCT into your research. Xu, the little horses are finally crossing this river. Berrend, Martijn en Leah, zonder de Biertuin-avonden was het sowieso niet gelukt.

Martijn, dr. de Bruin, bedankt voor je motivational one-liners, support en aanmoediging. Ik heb enorm veel van je geleerd. Bedankt dat je me hebt geïntroduceerd bij de COST bijeenkomsten; dat waren een paar mooie meetings en reisjes. Ik ben benieuwd naar alle awesome dingen die je in de toekomst gaat doen.

Sanne, wat fijn dat we een kamer op het AMC hebben gedeeld en zo elkaar beter hebben leren kennen. Ik heb genoten van onze gesprekken, conferenties en onze samenwerking aan het artikel dat ook de weg naar dit boekje heeft gevonden. Sparkle B.V. wordt heus nog wel een ding!

Beste Paul, high five... it's done! In het lab werken met jou was altijd een klein feestje. Van woordgrappen, lijstjes, awesome optische constructies (the flip mode mirror) tot whiskey avondjes (Writer's tears). We hadden natuurlijk ook tegenslagen, eigenlijk vooral één: dispersie compensatie. Maar bovenal was jouw bijna oneindige kennis over optische systemen altijd zeer waardevol.

Beste Martin Brandt, bedankt voor het meedenken en meewerken aan de automatisering van de OCT analyses. Ik ben trots op onze samenwerking waarmee we de EYR prijs van SURF hebben binnen gesleept. The collaboration and connection that followed with SURF and eScience Center were inspiring and fun. Cheers Jan!

Beste Carla, ontzettend bedankt voor je enthousiaste behulpzaamheid en het regelwerk om onze promoties daadwerkelijk tot stand te laten komen.

I am grateful for my experiences during the Recess college activities. Special thanks to everyone that made it possible and everyone I connected with.

Beste paranimfen, Leah, Arnie. Ontzettend fijn dat jullie mijn paranimfen willen zijn. Ik kan me geen beter paranimf-duo voorstellen. In mijn venndiagram van wetenschappelijke en maatschappelijke discussies, muziek en bier, staan jullie in het overlappende deel. Dank jullie wel! Arnie, van café Lekker Belangrijk tot hier, ik denk dat ik er weinig

aan toe hoeft te voegen. Thanks! Dear Leah, thank you for being you, and such an amazing colleague and friend. I am truly grateful and enjoyed all the projects we tackled together with your mad Matlab skills, scientific insight and support.

Studiemaatjes: Arthur, Esther, Vincent en Freek. Bedankt voor de leuke filmavonden en frustratie-deel-biertjes. Rens, dank je voor je support en al je ongezoete adviezen.

Lieve lieve vrienden... al kan ik onmogelijk iedereen hier noemen, ik bof met zulke fijne mensen om me heen! Lutsers, Marlice, Angelique, Inge, Hester, Raül, Wesley, Rob en Paul, ontzettend veel dank voor de liefde, gezelligheid, feestjes en oneindige support. James, thank you for the cover and lay-out design, it's spot on!

Lieve Sander, bedankt voor je positiviteit en aanmoediging. Ik ben blij dat ik de laatste fase van het tot stand komen van dit boekje met je heb kunnen delen. Op naar het volgende avontuur!!